DR. MICHEL VAN WEEGHEL (Orcid ID : 0000-0002-4916-2866)

Article type : Original

Title

Hepatic ChREBP activation limits NAFLD development in a mouse model for Glycogen Storage Disease type Ia

Author names

Yu Lei[1], Joanne A. Hoogerland[1], Vincent W. Bloks[1], Trijnie Bos[2], Aycha Bleeker[1], Henk Wolters[1], Justina C. Wolters[1], Brenda S. Hijmans[1], Theo H. van Dijk[2], Rachel Thomas[3], Michel van Weeghel[4,5], Gilles Mithieux[6,7,8], Riekelt H. Houtkooper[4], Alain de Bruin[1,3], Fabienne Rajas[6,7,8], Folkert Kuipers[1,2] and Maaike H. Oosterveer[1]

Keywords

Glycogen Storage Disease type Ia, ChREBP, Non-Alcoholic Fatty Liver Disease, VLDL-TG secretion, TM6SF2

Contact information

Departments of [1]Pediatrics and [2]Laboratory Medicine, University of Groningen, University Medical Center Groningen, The Netherlands. [3]Dutch Molecular Pathology Center, Faculty of Veterinary Medicine, Utrecht University, 3584 CL Utrecht, The Netherlands. [4]Laboratory Genetic Metabolic Diseases, Amsterdam Gastroenterology and Metabolism, Amsterdam Cardiovascular Sciences, and [5]Core Facility Metabolomics, Amsterdam UMC, University of Amsterdam, Meibergdreef 9, Amsterdam, The Netherlands. [6]Institut National de la Santé et de la Recherche Médicale, U1213, Lyon, F-69008, [7]Université de Lyon, Lyon, F-69008 and [8]Université Lyon 1, Villeurbanne, F-69622, France.

Email addresses:

a74579@qq.com, j.a.hoogerland@umcg.nl, v.w.bloks@umcg.nl, t.bos01@umcg.nl, a.bleeker01@umcg.nl, h.wolters@umcg.nl, justina.c.wolters@rug.nl, brenda.hijmans@gmail.com, t.van.dijk@umcg.nl, r.e.thomas@uu.nl, m.vanweeghel@amc.uva.nl, gilles.mithieux@univ-lyon1.fr, r.h.houtkooper@amc.uva.nl, a.debruin@uu.nl, fabienne.rajas@univ-lyon1.fr, f.kuipers@umcg.nl, m.h.oosterveer@umcg.nl

List of Abbreviations

ALDO, aldolase; ALT, alanine aminotransferase; AST, aspartate aminotransferase; ChREBP, carbohydrate response element binding protein; CE, cholesteryl ester; DGAT, diacylglycerol acetyltransferase; ER, endoplasmic reticulum; F1,6bisP, fructose 1,6-bisphosphate; F6P/F1P, fructose-6/1-phosphate; FC, free cholesterol; G6P, glucose-6-phosphate; G6PC, glucose-6-phosphatase; DHAP/GAP, dihydroxyacetone phosphate/ glyceraldehyde-3-phosphate; GPI, G6P isomerase; GSD Ia/b, glycogen storage disease type Ia/b; H&E, Hematoxylin and eosin; HNF-4α, hepatocyte nuclear factor 4 alpha, MTTP, microsomal triglyceride transfer protein; NAFLD, non-alcoholic fatty liver disease; NAS, NAFLD activity score; ORO, Oil-red-O; PEP, phosphoenolpyruvate; PKLR, pyruvate kinase; PPP, pentose phosphate pathway; TG, triglyceride; TM6SF2, transmembrane 6 superfamily member 2; VLDL, very-low density lipoprotein.

Financial support

This work was supported by The Abel Tasman Talent Program (ATTP) of the University of Groningen to Y. Lei. M. H. Oosterveer is the recipient of a VIDI grant from the Dutch Scientific

Organization, and holds a Rosalind Franklin Fellowship from the University of Groningen. F. Kuipers is supported by CardioVasculair Onderzoek Nederland (IN-CONTROL II, CVON2018-27). J.C. Wolters is supported by Transcard (FP7-603091). F. Rajas and G. Mithieux are supported by the French National Research Agency (ANR-11-BSV1-009).

Abstract (275/275 words)

Glycogen storage disease type Ia (GSD Ia) is an inborn error of metabolism caused by defective glucose-6-phosphatase (G6PC) activity. GSD Ia patients exhibit severe hepatomegaly due to glycogen and triglyceride (TG) accumulation in the liver. We have previously shown that the activity of Carbohydrate Response Element Binding Protein (ChREBP), a key regulator of glycolysis and *de novo* lipogenesis, is increased in GSD Ia. In the current study we assessed the contribution of ChREBP to non-alcoholic fatty liver disease (NAFLD) development in a mouse model for hepatic GSD Ia. Liver-specific *G6pc* knockout (L-*G6pc*$^{-/-}$) mice were treated with AAV2/8-shChREBP to normalize hepatic ChREBP activity to levels observed in wildtype (L-*G6pc*$^{+/+}$) mice receiving AAV8-shScramble. Hepatic ChREBP knockdown markedly increased liver weight and hepatocyte size in L-*G6pc*$^{-/-}$ mice. This was associated with hepatic accumulation of G6P, glycogen and lipids, while the expression of glycolytic and lipogenic genes was reduced. Enzyme activities, flux measurements, hepatic metabolite analysis and VLDL-TG secretion assays revealed that hepatic ChREBP knockdown reduced downstream glycolysis and *de novo* lipogenesis, but also strongly suppressed hepatic VLDL lipidation hence promoting the storage of 'old fat'. Interestingly, enhanced VLDL-TG secretion in shScramble-treated L-*G6pc*$^{-/-}$ mice associated with a ChREBP-dependent induction of the VLDL lipidation proteins MTTP and TM6SF2, the latter being confirmed by ChIP-PCR. **Conclusion**: Attenuation of hepatic ChREBP induction in GSD Ia liver aggravates hepatomegaly due to further accumulation of glycogen and lipids as a result of reduced glycolysis and suppressed VLDL-TG secretion. TM6SF2, critical for VLDL formation, was identified as a novel ChREBP target in mouse liver. Altogether, our data show that enhanced ChREBP activity limits NAFLD development in GSD Ia by balancing hepatic TG production and -secretion.

Glycogen storage disease type Ia and Ib (GSD Ia/Ib) are rare, monogenetic disorders of carbohydrate metabolism. GSD Ia is caused by mutations in the glucose-6-phoshatase (G6PC) gene, while the glucose-6-phosphate (G6P) transporter (*SLC37A4*) gene is affected in GSD Ib (1). Impaired G6PC activity in hepatocytes, kidney cells and enterocytes of GSD Ia patients reduces endogenous glucose production, primarily contributing to fasting hypoglycemia. The intracellular accumulation of G6P, in turn, promotes glycogen synthesis, glycolysis and *de novo* lipogenesis. As a consequence, GSD Ia patients suffer from severe hepatomegaly and non-alcoholic fatty liver disease (NAFLD) and, strikingly, more than two-thirds of the patients develop liver tumors as young adults (2).

Carbohydrate Response Element Binding Protein (ChREBP, also known as MONDOB, MLXIPL or WBSCR14) is the main glucose-sensitive transcription factor in hepatocytes (3-5). ChREBP is activated in response to increased intracellular glucose metabolism, partly via glucose-dependent O-linked glycosylation and/or acetylation (6-8). In addition, nuclear localization of ChREBP is regulated by phosphorylation (6, 9) and its interaction with 14-3-3 proteins and importins (10, 11). The glucose-mediated activation of the canonical ChREBP isoform (ChREBP-α) induces the expression of ChREBP-β, a transcriptionally highly active isoform, hence generating a potent feed forward loop (12). In hepatocytes, ChREBP targets genes encoding enzymes involved in glycolysis, the pentose phosphate pathway (PPP), *de novo* lipogenesis as well as very-low density lipoprotein (VLDL) assembly (3, 4, 13). Thus, hepatic ChREBP allows for proper accommodation of glucose availability to its intracellular fates in metabolism, storage and redistribution in the form of lipids.

Previous work from our groups and others has shown that G6P accumulation in the liver of GSD Ia and GSD Ib mouse models strongly promotes hepatic ChREBP activity (14-16). Moreover, we have shown that the induction of glycolytic and lipogenic genes in acute GSD Ib critically depends on hepatic ChREBP expression (14). It has been reported that hepatic ChREBP is also activated in type 2 diabetic mice and that hepatic ChREBP knockdown in these animals protects against NAFLD (17, 18). In light of the association between hepatic ChREBP activity and NAFLD and the link between NAFLD and advanced liver disease risk, in the current study we evaluated the metabolic consequences of enhanced hepatic ChREBP activity in GSD Ia. For this purpose, we aimed to normalize hepatic ChREBP activity in a hepatocyte-specific model for GSD Ia. Surprisingly, our data show that attenuation of hepatic ChREBP induction in GSD Ia liver aggravated hepatomegaly as a result of reduced downstream glycolysis and lower VLDL-TG secretion, indicating that enhanced ChREBP activity limits hepatomegaly and NAFLD development in GSD Ia.

Experimental procedures

Animals

Male adult (13-18 weeks) *G6pc* floxed *Alb*-Cre negative (B6.*G6pc*$^{lox/lox}$) and *G6pc* floxed *Alb*-Cre positive (B6.*G6pc*$^{lox/lox}$.SA$^{creERT2/w}$ mice) (19) on a C57BL/6J background were housed in a light- and temperature-controlled facility (lights on 7AM-7PM) and fed a standard laboratory chow diet (RMH-B, Abdiets, Woerden). They were infected with shRNAs directed against ChREBP (AAV-ChREBP) or a scrambled control (AAV-Scramble) AAV-shScramble viruses (1 x 10^{12} particles per mouse) by intravenous injection into the retro-orbital plexus under isoflurane anesthesia. For a detailed description of the production, purification and titration of the AAV2/8 viruses, see the Supplementary Material. Twelve days after AAV-shRNA administration, all mice received i.p. injections of tamoxifen for 5 consecutive days to excise *G6pc* exon 3 (19), hence generating liver-specific *G6pc*-deficient mice (L-*G6pc*$^{-/-}$) and wildtype littermates (L-*G6pc*$^{+/+}$). Nonfasted animals were either sacrificed for tissue collection, or subjected to VLDL-TG secretion experiments, starting at 8AM 10 days after the last tamoxifen injection. Animals were sacrificed by cardiac puncture under isoflurane anesthesia and tissues were rapidly excised and stored.

Ex vivo lipolysis

Epididymal white adipose tissue was removed and stored on ice in Krebs buffer (12 mM HEPES, 4.9 mM KCl, 121 mM NaCl, 1.2 mM $MgSO_4$, 0.33 mM $CaCl_2$, 0.1% glucose and 3.5% fatty acid free BSA, pH 7.4) until further processing. Tissue samples were incubated in Krebs buffer (10% w/v) at 37°C. After 1, 2, 3 and 4 hours of incubation, independent samples were centrifuged at maximum speed, and supernatants were collected for glycerol analysis using a commercially available kit (Cayman Chemical, Ann Arbor, MI, USA).

Histological and pathological analysis of the liver

For microscopic examination, tissues were fixed in 4% (wt/v) formaldehyde in PBS, embedded in paraffin, sectioned at 4 µm, and stained with Hematoxilin&Eosin and Periodic Acid Schiff (PAS). Liver steatosis was visualized by Oil red O staining of liver cryosections. Photomicrographs of five areas per section of liver were made at 200x magnification using the Olympus DP26 camera with Olympus cellSens™ Standard software (v1.18). To perform digital image analysis, an imageJ (v1.50, National Institutes of Health, Bethesda, MD) macro script was created to assess the extent of lipid staining (total area and lipid droplet size). Hepatic steatosis was assessed blindly and graded in H&E-stained liver sections using an adapted version of the NAFLD activity scoring (NAS) system developed by Kleiner *et al* (20).

Biochemical assays

Blood glucose was measured using a One Touch Ultra glucose meter (Life-Scan Inc.). Plasma insulin, glucagon, lactate, ketone bodies, free fatty acids, triglycerides and cholesterol were analyzed using commercially available ELISA kits (Chrystal Chem, Alpco Diagnostics, Instruchemie, Wako, DiaSys and Roche respectively). Hepatic glycogen and G6P content was determined as previously described (14).

Hepatic lipid, acylcarnitine and metabolome analysis

The procedures for quantification of lipid, acylcarnitine and metabolome profiles in liver homogenates are described in the Supplementary Material.

Glycolytic enzyme capacities (V_{max})

The hepatic activities of glyceraldehyde 3-phosphate dehydrogenase (GAPDH), phosphoglucose isomerase (GPI), aldolases (ALDO; in liver mainly ALDO A&B), enolases (ENO; in liver mainly ENO1&3) and pyruvate kinase (LPK) were determined *ex vivo* in liver homogenates as described in the Supplementary Material.

Quantification of acetyl-CoA precursor pool enrichments, *de novo* lipogenesis, fatty acid elongation and cholesterol synthesis

These procedures are described in the Supplementary Material.

Gene expression analysis

The procedures for quantification of hepatic RNA expression levels are described in the Supplementary Material.

Targeted proteomics

The procedures for targeted proteomics are described in the Supplementary Material.

***In silico* predictions**

These procedures are described in the Supplementary Material.

ChIP-qPCR on the mouse *Tm6sf2* promoter

In order to acutely induce hepatic GSD Ib, male C57BL/6J mice were equipped with a permanent catheter in the right jugular vein for infusions and were allowed a recovery period of at least 4 days. Animals were kept in experimental cages during the experiment and the preceding fasting period, allowing frequent collection of tail blood samples. After overnight fasting, mice were infused for 6 hours with S4048 (a generous gift from Sanofi-Aventis, Germany, 5.5 mg/mL PBS with 6% DMSO at 0.135 mL/h) or vehicle. After 6 hours, mice were sacrificed by cardiac puncture. For fasting/feeding studies, male C57BL6/J mice were sacrificed by cardiac puncture (8:00 AM) in either a fed or a 9-hour fasted (11:00 PM - 8:00 AM) state. Livers from S4048 or vehicle-treated as well as fasted/fed mice were harvested for ChIP-qPCR analysis which was performed as described in the Supplementary Material.

VLDL-TG secretion rates and nascent VLDL analysis

Mice were injected intraperitoneally with Poloxamer 407 (1 g/kg body weight). Blood samples (50 μL) were drawn under isoflurane anesthesia by retro-orbital bleeding into heparinized tubes at 0, 30, 60, 120, and 240 minutes after injection. After sampling the bleeding was immediately stopped upon slight compression with sterile gauze to minimize additional blood loss. Plasma was isolated by centrifugation after which TG levels and TG secretion rates were determined as described (4). For isolation and analysis of nascent VLDL, see Supplementary Material.

Cell reporter assays

The cell reporter assays are described in the Supplementary Material.

Statistics

Data in figures is presented as box and-whisker plots indicating the sample minimum, lower quartile, median, upper quartile, and sample maximum, or in some cases data is presented as mean ± SEM. Data in heatmaps represent z-score normalized values. Statistical analysis was performed using BrightStat software. Differences between two or multiple groups were tested by Mann-Whitney U-test or Kruskal-Wallis H-test followed by post-hoc Conover pairwise comparisons, respectively. p-values <0.001 (*** or ^^^), 0.001 to 0.01 (**, ^^ or ##), and 0.01 to 0.05 (*, ^ or #) were considered significant.

Results

Hepatic ChREBP knockdown reduces downstream glycolysis and increases hepatic G6P and glycogen storage in L-G6pc$^{-/-}$ mice

To evaluate the consequences of normalized hepatic ChREBP activity in L-*G6pc*$^{-/-}$ mice, we administered a short hairpin (sh)RNA against ChREBP*α*/*β* or a scrambled shRNA to L-*G6pc*$^{+/+}$ and L-*G6pc*$^{-/-}$ mice by means of adeno-associated virus delivery. Hepatic *Chrebpα* mRNA levels remained unaffected upon shRNA administration in L-*G6pc*$^{+/+}$ mice, but were reduced by ~40% in L-*G6pc*$^{-/-}$ mice (Fig. 1A). The hepatic mRNA expression levels of *Chrebpβ*, the key marker of ChREBP activity (12, 21), were similarly (~40%) reduced in in L-*G6pc*$^{+/+}$ and L-*G6pc*$^{-/-}$ mice, hence normalizing its expression in L-*G6pc*$^{-/-}$ mice to the levels observed in L-*G6pc*$^{+/+}$ controls receiving scrambled shRNA (Fig. 1A). Hepatic G6PC protein abundance was strongly reduced in L-*G6pc*$^{-/-}$ mice receiving either of the two shRNAs (Fig. 1A). ChREBP*α*/*β* protein abundance was reduced by about 50% in shChREBP as compared to scramble shRNA-treated mice of either genotype (Fig. 1A). Consistent with reduced hepatic ChREBP activity, the mRNA expression (Fig. 1B; upper panel) and enzymatic activities (Fig. 1C) of the established glycolytic ChREBP targets (3-5, 22) G6P isomerase (*Gpi*), aldolase B (*Aldob*) and pyruvate kinase (*Pklr*), were normalized by shChREBP in L-*G6pc*$^{-/-}$ mice. These reductions in glycolytic enzyme activities were paralleled by a more pronounced accumulation of the glycolytic intermediates G6P, fructose-6/1-phosphate (F6P/F1P) and fructose-1,6-bisphosphate (F1,6bisP) in the liver of shChREBP versus shScramble-treated L-*G6pc*$^{-/-}$ mice, while there was no significant accumulation of hepatic triose phosphates (DHAP/GAP), phosphoenolpyruvate (PEP), pyruvate or lactate between these groups (Fig. 1D; upper panel). On the contrary, hepatic ChREBP knockdown did further increase hepatic 6-phosphogluconolactone, gluconate-6P, xylulose-5-phosphate and sedoheptulose-7P content in L-*G6pc*$^{-/-}$ mice, showing that shChREBP also resulted in more pronounced accumulation of oxidative PPP intermediates as compared to shScramble treated mice while ribose-5-phosphate/ribulose-5-phosphate, ribose-1,5-disphosphate and 2-dehydrogluconate-6-phosphate were not affected (Fig. 1D; lower panel). Moreover, we observed that ChREBP knockdown increased relative and total hepatic glycogen contents in L-*G6pc*$^{-/-}$ versus L-*G6pc*$^{+/+}$ mice (Fig. 1E). Body weight and food intake were similar in all groups (Table 1). Liver weight was significantly increased in shChREBP- versus shScramble-treated L-*G6pc*$^{+/+}$ and L-*G6pc*$^{-/-}$ mice, although hepatic water content was reduced upon ChREBP knockdown in both genotypes and hepatic protein content was specifically reduced in shChREBP-treated L-*G6pc*$^{-/-}$ mice as compared to shScramble-treated mice with the same genotype (Table 1). Plasma ALT and AST levels were elevated in shScramble-treated L-*G6pc*$^{-/-}$ as compared to L-*G6pc*$^{+/+}$ mice and further

increased upon hepatic ChREBP knockdown in L-*G6pc*$^{-/-}$ mice (Table 1). Blood glucose and plasma insulin concentrations were reduced in shChREBP treated L-*G6pc*$^{-/-}$ mice, while plasma lactate concentrations were not affected by hepatic *G6pc* deficiency and/or ChREBP knockdown (Table 1).

Hepatic ChREBP knockdown promotes hepatic lipid storage but reduces fractional de novo lipogenesis in L-G6pc$^{-/-}$ *mice*

Hematoxylin and eosin (H&E) staining of the livers showed that hepatic ChREBP knockdown resulted in marked hepatocyte vacuolation in both L-*G6pc*$^{-/-}$ and L-*G6pc*$^{+/+}$ mice (Fig. 2A). Besides glycogen accumulation, cytoplasmic vacuolation can result from excess lipid storage. Oil-red-O (ORO) staining for neutral lipids indeed showed increased deposition of neutral lipids in shChREBP versus shScramble-treated groups of both genotypes (Fig. 2A). Quantification of the lipid droplet size showed that the droplets in shChREBP-treated groups were enlarged (Fig. 2A). Accordingly, the NAFLD activity scores (NAS; (20)) indicated that hepatic ChREBP knockdown induced fatty liver disease in L-*G6pc*$^{+/+}$ mice, while it aggravated the existing fatty liver in L-*G6pc*$^{-/-}$ mice (Fig. 2B). Biochemical analysis of the hepatic lipids revealed that hepatic ChREBP knockdown resulted in substantial increases in the contents and total amounts of hepatic TGs and cholesteryl esters (CEs) (Fig. 2B), while total hepatic free cholesterol (FC) and phospholipid content were similarly increased in shScramble and shChREBP-treated L-*G6pc*$^{-/-}$ mice as compared to their wildtype controls (Fig. S1A). As expected, hepatic ChREBP knockdown reduced the mRNA expression of hepatic fatty acid synthesis genes as well as that of acylCoA:diacylglycerol acetyltransferase 1 and 2 (*Dgat1/2*) (Fig. 2C) hence normalizing their expression levels in L-*G6pc*$^{-/-}$ mice to values observed in shScramble-treated L-*G6pc*$^{+/+}$ mice. On the other hand, neither hepatic G6PC deficiency nor Chrebp knockdown consistently altered the mRNA levels of the other TG synthesis enzymes (Fig. 2C). ^{13}C-labeled acetate was administered to quantify *de novo* lipogenesis and fatty acid elongation (23). Fractional acetyl-CoA pool enrichments, determined from ^{13}C-incorporation in hepatic palmitate (C16:0) and palmitoleate (C16:1), were reduced in both groups of L-*G6pc*$^{-/-}$ mice as well as in shChREBP-treated L-*G6pc*$^{+/+}$ mice (Fig. 2D), indicating changes in acetyl-CoA pool turnover under these conditions. Moreover, subsequent quantification of lipogenic fluxes revealed that hepatic ChREBP knockdown reduced fractional *de novo* lipogenesis in both L-*G6pc*$^{+/+}$ and L-*G6pc*$^{-/-}$ mice, with the largest effects seen on *de novo* oleate (C18:1) synthesis (Fig. 2E). On the other hand, elongation of pre-existing palmitate was exclusively reduced by shChREBP treatment of L-*G6pc*$^{-/-}$ mice (Fig. 2E). Interestingly, despite these reductions in fractional lipogenesis, absolute rates of *de novo* lipogenesis and chain elongation were slightly increased in shChREBP treated L-*G6pc*$^{-/-}$ mice as

compared to their shScramble-treated controls (Fig. 2F). However, in quantitative terms, these increases were marginal as compared to the storage of pre-existing fatty acids, referred to as 'old fat', which was markedly increased upon hepatic ChREBP knockdown in both genotypes (Fig. 2F, Table 2).

Hepatic ChREBP knockdown strongly suppresses hepatic VLDL-TG secretion by reducing VLDL-TG lipidation

To establish the origin of the old fat accumulating upon hepatic ChREBP knockdown, we analyzed fatty acid oxidation, adipose tissue lipolysis and hepatic VLDL-TG secretion pathways. We observed that hepatic C2-acylcarnitine content was increased, while lauroleate (C12:1)-, palmitoleate (C16:1)- and oleate (C18:1)-acylcarnitines were reduced in the livers of shChREBP- versus shScramble-treated L-*G6pc*$^{-/-}$ mice, suggesting increased fatty acid oxidation upon hepatic ChREBP knockdown in L-*G6pc*$^{-/-}$ mice (Table 3). Plasma ketone body concentrations were, however, not affected by hepatic G6PC deficiency and/or ChREBP knockdown (Table 1). Quantification of adipose tissue lipolysis *ex vivo* revealed no differences as a consequence of hepatic *G6pc* deficiency and/or ChREBP knockdown (Fig. S2A), while circulating NEFA levels were increased in shScramble and shChREBP-treated L-*G6pc*$^{-/-}$ mice versus their wildtype controls (Table 1). Interestingly, total plasma TG levels (Table 1) and VLDL-TG levels (Fig. 3A) were elevated in shScramble-treated L-*G6pc*$^{-/-}$ as compared to L-*G6pc*$^{+/+}$ mice but reduced upon hepatic ChREBP knockdown in mice of both genotypes. In parallel, we observed a marked reduction of VLDL-TG secretion rates (Fig. 3B) upon hepatic ChREBP knockdown, both in L-*G6pc*$^{+/+}$ and L-*G6pc*$^{-/-}$ mice. Moreover, the nascent VLDL particles of shChREBP-treated mice contained less TGs, resulting in a marked decrease in VLDL particle volume (Fig. 3C). The smaller VLDL particle volume upon hepatic ChREBP knockdown was confirmed by Western Blot analysis showing reductions in the TG/APOB ratio upon shChREBP treatment, which was strongest in L-*G6pc*$^{-/-}$ mice (Fig. 3C and S2B).

ChREBP regulates hepatic MTTP and TM6SF2 expression

VLDL particles are assembled by lipidation of APOB in the endoplasmic reticulum (ER) and Golgi, mediated by microsomal triglyceride transfer protein (MTTP) and transmembrane 6 superfamily member 2 (TM6SF2). As expected (3, 13), we observed that hepatic ChREBP knockdown reduced hepatic *Mttp* mRNA (Fig. 4A) and protein abundance (Fig. 4B) in L-*G6pc*$^{+/+}$ and L-*G6pc*$^{-/-}$ mice. Interestingly, we observed that also *Tm6sf2* mRNA levels and -protein abundance were induced in shScramble treated L-*G6pc*$^{-/-}$ mice as compared to wildtype controls, and normalized in shChREBP-treated L-*G6pc*$^{-/-}$ mice (Fig. 4A and 4B). We confirmed that *Tm6sf2* mRNA levels

were also ChREBP-dependently induced in mice treated with the G6P transporter SLC37A4 inhibitor S4048 (Fig. 4C), an acute model for hepatic GSD Ib (14). Publicly available liver ChREBP ChIP-seq data (4) indicated potential regulation of *Tm6sf2* by ChREBP, and computational analysis revealed four putative ChREBP binding sites in the mouse *Tm6sf2* promoter (Fig. 4D). ChIP-qPCR analysis showed specific recruitment of ChREBP to these binding sites upon S4048 treatment, indicating that hepatic ChREBP directly controls murine *Tm6sf2* transcription (Fig. 4D). Moreover, analysis of publicly available gene expression data (GSE61576, (24)) revealed that hepatic ChREBP overexpression induced *Tm6sf2* expression in mouse liver (Fig. S3A). Cell reporter assays indicated that ChREBPα/MLX and ChREBPβ/MLX further enhanced the transactivation of the mouse *Tm6sf2* gene reporter by hepatocyte nuclear factor 4 alpha (HNF-4α), while they did not transactivate the reporter in the absence of HNF-4α (Fig. 4E). Finally, ChIP-qPCR analysis of mouse liver indicated that both ChREBP and HNF-4α are associated with the *Tm6sf2* promoter, and that these interactions are significantly higher in fed versus fasted mice (Fig. 4F).

Discussion

Patients with glycogen storage disease type Ia (GSD Ia) experience severe hepatomegaly and develop NAFLD. We have previously shown that hepatic activity of the glucose-sensitive transcription factor ChREBP is increased in mouse models for GSD Ia and GSD Ib and ChREBP mediates the induction of glycolytic and lipogenic genes in acute GSD Ib (14, 15). As enhanced glycolysis and lipogenesis promote hepatic lipid storage, these findings prompted us to evaluate the contribution of enhanced ChREBP activity to the development of NAFLD in GSD Ia mice. We found that normalization of hepatic ChREBP activity in L-*G6pc*$^{-/-}$ mice by shRNA-mediated knockdown, as validated by the expression of the key marker gene *Chrebpβ* (12, 21), further promoted hepatomegaly, hepatocyte vacuolation and NAFLD development due to additional accumulation of glycogen and lipids in the liver. Notably, aggravation of NAFLD in shChREBP-treated L-*G6pc*$^{-/-}$ mice occurred despite a reduction in fractional *de novo* lipogenesis, and was associated with a marked suppression of hepatic VLDL-TG secretion. These changes were paralleled by a ChREBP-dependent reduction in hepatic expression of MTTP and TM6SF2, proteins that are both involved in VLDL lipidation (25). Interestingly, we also observed that ChREBP was recruited to the murine *Tm6sf2* promoter in response to hepatic G6P accumulation, thereby identifying TM6SF2 as a transcriptional target of ChREBP in mouse liver under conditions of increased intracellular glucose signaling. Altogether, our data indicate that enhanced hepatic ChREBP activity limits hepatomegaly, hepatocyte vacuolation and NAFLD development in GSD Ia, and should therefore be considered as a 'protective' response under these conditions of excessive intrahepatic glucose metabolism.

NAFLD results from an imbalance between hepatic TG input and –output, and 'snapshot' hepatic TG content is therefore determined by hepatic FFA influx rates, the activities of *de novo* lipogenesis and fatty acid oxidation pathways as well as VLDL-TG secretion (26). The activities and relative contributions of these processes may change under different physiological (e.g. feeding and fasting conditions) and disease states (e.g. obesity and diabetes). As ChREBP exerts transcriptional control on the expression of key genes involved in *de novo* lipogenesis, fatty acid oxidation and VLDL-TG secretion (3-5, 13, 27), the consequence of altered hepatic ChREBP activity for NAFLD development is likely dependent on the prevailing (patho)physiological condition. Previous research has shown that partial or complete ablation of ChREBP reduces hepatic lipid content in type 2 diabetic mice (17, 18), a well as in some (28, 29), but not all (30, 31) studies in which rodents were fed carbohydrate or fructose-rich diets. On the other hand,

ChREBP inactivation did not lower hepatic lipid content under conditions of chow or high-fat feeding (13, 28, 32). In the current study, we demonstrate that normalization of ChREBP activity in GSD Ia hepatocytes suppresses fractional *de novo* lipogenesis while elevated hepatic C2-acylcarnitine levels under these conditions are indicative of enhanced hepatic fatty acid oxidation. Yet hepatic accumulation of 'old fat' was increased in shChREBP-treated mice, due to a strong suppression of VLDL-TG secretion. Thus, the reduction in *de novo* fatty acid synthesis and the increase in fatty acid catabolism were insufficient to compensate for reduced VLDL lipidation and –secretion in 'our disease context', i.e., (non-fasted) normoglycemic L-*G6pc*$^{-/-}$ mice. The fractional contribution of hepatic *de novo* fatty oleate synthesis in L-*G6pc*$^{-/-}$ mice was limited and reduced from ~20% to ~10% upon hepatic ChREBP knockdown (Fig. 2E). As a consequence, total hepatic *de novo* oleate synthesis was reduced by 5 µmoles in shChREBP versus shScramble treated L-*G6pc*$^{-/-}$ mice within the 48 hours of ^{13}C-acetate administration. On the other hand, VLDL-TG secretion was reduced by about 350 µmol/kg/h upon hepatic ChREBP knockdown (Fig. 3B), corresponding to a reduction in hepatic oleate export of about 10 µmol per hour. Thus, indeed, the amount of excess fatty acids stored in liver due to impaired VLDL-TG secretion massively exceeded the shChREBP-mediated reduction in *de novo* fatty acid synthesis. In contrast to L-*G6pc*$^{-/-}$ mice, which show a ~60% increase in VLDL-TG secretion rate as compared to wildtype controls (Fig. 3B), our laboratory has previously shown that VLDL-TG secretion is unchanged in type 2 diabetic mice compared to controls (33). As a result, the excess storage of 'old fat' due to suppression of VLDL-TG secretion in response to hepatic ChREBP knockdown is likely of less quantitative importance in type 2 diabetes as compared to L-*G6pc*$^{-/-}$ mice. Moreover, fractional palmitate synthesis accounts for ~50% in chow-fed type 2 diabetic mice (33) versus 30% in L-*G6pc*$^{-/-}$ mice (Fig. 2E), while the contribution of hepatic NEFA influx may be larger in obese insulin-resistant mice as compared to L-*G6pc*$^{-/-}$ mice (26, 34). Therefore the differential contributions of *de novo* lipogenesis and VLDL-TG secretion to hepatic lipid content likely explain most of the opposing effects of hepatic ChREBP inhibition on lipid accumulation in type 2 diabetic (17, 18) versus hepatocyte-specific GSD Ia mice. Besides the variable efficacies of hepatic ChREBP knockdown between studies, we propose that differences in the contribution of *de novo* lipogenesis, VLDL-TG secretion and fatty acid oxidation pathways explain the reported divergent effects of hepatic ChREBP knockdown on NAFLD (13, 17, 18, 22, 28-31). Along similar lines, the observed increase in hepatic cholesterol synthesis and ER stress in high-fructose fed whole-body ChREBP knockout mice (29) is likely also context-dependent, as was proposed by Kim *et al*. (30). In contrast to what has been reported (29), hepatic ChREBP knockdown did not alter the expression of cholesterol biosynthesis genes (Fig. S1B) or fractional cholesterol synthesis rates in the livers of L-*G6pc*$^{-/-}$ mice in the current study (Fig. S1C). Absolute cholesterol synthesis was

only slightly increased in these animals (Fig. S1C). On the other hand, consistent with Zhang *et al*., (29) we did observe increased mRNA levels of ER stress markers *Bbc3* and *Ddit3* in shChREBP-treated L-*G6pc*$^{-/-}$ mice (Fig. S1D). Combined, published data and our current findings indicate that the relationship between hepatic ChREBP activity and NAFLD development is disease context-dependent.

Our study shows that ChREBP plays a key role in hepatic VLDL lipidation and –secretion in GSD Ia and is essential for proper regulation of hepatic TG balance and, consequently, NAFLD development under conditions of high intrahepatic glucose availability. Besides confirming the regulatory role of ChREBP in VLDL-TG production and -secretion (13, 31, 32), our work mechanistically supports genetic studies in humans that have linked ChREBP expression to plasma lipid levels (35-39). Our findings also establish the contribution of ChREBP activity to enhanced VLDL-TG secretion and hypertriglyceridemia in GSD Ia (Hoogerland *et al*., unpublished). Importantly, our study identifies G6P-ChREBP signaling as a regulatory axis that controls TM6SF2 abundance in the liver under conditions of excessive intrahepatic glucose metabolism. Our molecular *in vivo* and *in vitro* studies indicate that HNF-4α contributes to regulation of basal Tm6sf2 transcription in mouse liver, while ChREBP mediates a glucose/G6P-induced induction of *Tm6sf2*. This potential mechanism is supported by strongly reduced hepatic *Tm6sf2* levels in hepatocyte-specific *Hnf-4*α knockout mice, and slightly lower in *Tm6sf2* expression in ChREBP null mice as compared to their wildtype littermates (Fig. S3E). TM6SF2 function was originally linked to human NAFLD in an exome-wide association study (40). Subsequent research has shown that its activity is essential for VLDL lipidation and maintenance of hepatic TG balance (40-44). However, to the best of our knowledge, this is the first study to report a HNF-4α/ChREBP-dependent induction of TM6SF2 abundance in response to G6P accumulation in mouse liver. Thus, besides regulating MTTP abundance (13), hepatic ChREBP also appears to regulate VLDL lipidation *via* TM6SF2. The impaired hepatic VLDL lipidation and suppression of hepatic TG secretion with comcomitant increases in hepatic TG content and lipid droplet size in shChREBP-treated L-*G6pc*$^{+/+}$ and L-*G6pc*$^{-/-}$ mice in the current study actually phenocopies what has been observed upon hepatic *Tm6sf2* knockdown and in *Tm6sf2* knockout mice (40-42). In contrast to synergistic effect of ChREBP and HNF-4α on murine *Tm6sf2* reporter activation, ChREBPα and -β did not promote HNF-4α-induced transactivation of the human *TM6SF2* gene reporter (Fig. S3D). However, the reporter gene used does not cover all predicted ChREBP and HNF-4α binding sites in the human TM6SF2 gene (Fig. S3B). Whether or not

ChREBP and HNF-4α also cooperatively regulate of hepatic *TM6SF2* expression in human hepatocytes can therefore not be concluded from our studies. Yet, in view of the similarities in liver pathophysiology between GSD Ia and type 2 diabetes (45, 46), it is tempting to speculate that a ChREBP-dependent induction of hepatic *TM6SF2* potentially also contributes to hypertriglyceridemia in type 2 diabetics (47, 48). Follow-up research will be essential to assess the translational value to our newly identified regulatory mechanism.

In conclusion, our study shows that hepatic ChREBP maintains TG balance in GSD Ia liver by concomitantly regulating hepatic lipogenesis, fatty acid oxidation and particularly VLDL-TG secretion (3-5, 13, 27), thereby limiting NAFLD development. Our work identifies hepatic G6P-ChREBP signaling as a novel regulatory axis that controls murine TM6SF2 expression, hence controlling VLDL-lipidation and -secretion. Enhanced ChREBP activity also likely protects against NAFLD progression to advanced liver disease under conditions of excessive hepatic glucose metabolism, such as GSD Ia and type 2 diabetes.

Acknowledgements

We thank W. Liu, N.L, Mulder, W. Bin Obaid, I.A. Martini, M. H. Koster, K. van Eunen, A. Gerding, A. Jurdinski, R. Havinga for excellent technical assistance and D-J Reijngoud for scientific discussion. We thank A. Herling and D. Schmoll (Sanofi) for providing S4048, L. Chan for sharing the ChREBP ChIP-seq data set and Johan W. Jonker and Mark Herman for sharing HNF-4α and ChREBPα/β/Mlx expression plasmids.

References

1. Chou JY, Jun HS, Mansfield BC. Type I glycogen storage diseases: disorders of the glucose-6-phosphatase/glucose-6-phosphate transporter complexes. J Inherit Metab Dis 2014.
2. Rake JP, Visser G, Labrune P, Leonard JV, Ullrich K, Smit GP. Glycogen storage disease type I: diagnosis, management, clinical course and outcome. Results of the European Study on Glycogen Storage Disease Type I (ESGSD I). Eur J Pediatr 2002;161 Suppl 1:S20-34.
3. Ma L, Robinson LN, Towle HC. ChREBP center dot Mlx is the principal mediator of glucose-induced gene expression in the liver. Journal of Biological Chemistry 2006;281:28721-28730.
4. **Poungvarin N, Chang B, Imamura M, Chen J**, Moolsuwan K, Sae-Lee C, Li W, et al. Genome-Wide Analysis of ChREBP Binding Sites on Male Mouse Liver and White Adipose Chromatin. Endocrinology 2015;156:1982-1994.
5. Dentin R, Pegorier JP, Benhamed F, Foufelle F, Ferre P, Fauveau V, Magnuson MA, et al. Hepatic glucokinase is required for the synergistic action of ChREBP and SREBP-1c on glycolytic and lipogenic gene expression. Journal of Biological Chemistry 2004;279:20314-20326.
6. Dentin R, Tomas-Cobos L, Foufelle F, Leopold J, Girard J, Postic C, Ferre P. Glucose 6-phosphate, rather than xylulose 5-phosphate, is required for the activation of ChREBP in response to glucose in the liver. Journal of Hepatology 2012;56:199-209.
7. **Guinez C, Filhoulaud G**, Rayah-Benhamed F, Marmier S, Dubuquoy C, Dentin R, Moldes M, et al. O-GlcNAcylation increases ChREBP protein content and transcriptional activity in the liver. Diabetes 2011;60:1399-1413.
8. Bricambert J, Miranda J, Benhamed F, Girard J, Postic C, Dentin R. Salt-inducible kinase 2 links transcriptional coactivator p300 phosphorylation to the prevention of ChREBP-dependent hepatic steatosis in mice. J Clin Invest 2010;120:4316-4331.
9. Kawaguchi T, Takenoshita M, Kabashima T, Uyeda K. Glucose and cAMP regulate the L-type pyruvate kinase gene by phosphorylation/dephosphorylation of the carbohydrate response element binding protein. Proc Natl Acad Sci U S A 2001;98:13710-13715.
10. Sato S, Jung H, Nakagawa T, Pawlosky R, Takeshima T, Lee WR, Sakiyama H, et al. Metabolite Regulation of Nuclear Localization of Carbohydrate-response Element-binding Protein (ChREBP): ROLE OF AMP AS AN ALLOSTERIC INHIBITOR. J Biol Chem 2016;291:10515-10527.

11. Nakagawa T, Ge Q, Pawlosky R, Wynn RM, Veech RL, Uyeda K. Metabolite regulation of nucleo-cytosolic trafficking of carbohydrate response element-binding protein (ChREBP): role of ketone bodies. J Biol Chem 2013;288:28358-28367.
12. Herman MA, Peroni OD, Villoria J, Schon MR, Abumrad NA, Bluher M, Klein S, et al. A novel ChREBP isoform in adipose tissue regulates systemic glucose metabolism. Nature 2012;484:333-338.
13. Wu W, Tsuchida H, Kato T, Niwa H, Horikawa Y, Takeda J, Iizuka K. Fat and carbohydrate in western diet contribute differently to hepatic lipid accumulation. Biochem Biophys Res Commun 2015;461:681-686.
14. Grefhorst A, Schreurs M, Oosterveer MH, Cortes VA, Havinga R, Herling AW, Reijngoud DJ, et al. Carbohydrate-response-element-binding protein (ChREBP) and not the liver X receptor alpha (LXRalpha) mediates elevated hepatic lipogenic gene expression in a mouse model of glycogen storage disease type 1. Biochem J 2010;432:249-254.
15. Abdul-Wahed A, Gautier-Stein A, Casteras S, Soty M, Roussel D, Romestaing C, Guillou H, et al. A link between hepatic glucose production and peripheral energy metabolism via hepatokines. Mol Metab 2014;3:531-543.
16. Cho JH, Kim GY, Pan CJ, Anduaga J, Choi EJ, Mansfield BC, Chou JY. Downregulation of SIRT1 signaling underlies hepatic autophagy impairment in glycogen storage disease type Ia. PLoS Genet 2017;13:e1006819.
17. Iizuka K, Miller B, Uyeda K. Deficiency of carbohydrate-activated transcription factor ChREBP prevents obesity and improves plasma glucose control in leptin-deficient (ob/ob) mice. Am J Physiol Endocrinol Metab 2006;291:E358-364.
18. Dentin R, Benhamed F, Hainault I, Fauveau V, Foufelle F, Dyck JRB, Girard J, et al. Liver-specific inhibition of ChREBP improves hepatic steatosis and insulin resistance in ob/ob mice. Diabetes 2006;55:2159-2170.
19. Mutel E, Abdul-Wahed A, Ramamonjisoa N, Stefanutti A, Houberdon I, Cavassila S, Pilleul F, et al. Targeted deletion of liver glucose-6 phosphatase mimics glycogen storage disease type 1a including development of multiple adenomas. J Hepatol 2011;54:529-537.
20. Kleiner DE, Brunt EM, Van Natta M, Behling C, Contos MJ, Cummings OW, Ferrell LD, et al. Design and validation of a histological scoring system for nonalcoholic fatty liver disease. Hepatology 2005;41:1313-1321.
21. **Kim MS, Krawczyk SA**, Doridot L, Fowler AJ, Wang JX, Trauger SA, Noh HL, et al. ChREBP regulates fructose-induced glucose production independently of insulin signaling. J Clin Invest 2016;126:4372-4386.
22. Iizuka K, Bruick RK, Liang G, Horton JD, Uyeda K. Deficiency of carbohydrate response

element-binding protein (ChREBP) reduces lipogenesis as well as glycolysis. Proc Natl Acad Sci U S A 2004;101:7281-7286.
23. Oosterveer MH, van Dijk TH, Tietge UJ, Boer T, Havinga R, Stellaard F, Groen AK, et al. High fat feeding induces hepatic fatty acid elongation in mice. PLoS One 2009;4:e6066.
24. **Benhamed F, Denechaud PD**, Lemoine M, Robichon C, Moldes M, Bertrand-Michel J, Ratziu V, et al. The lipogenic transcription factor ChREBP dissociates hepatic steatosis from insulin resistance in mice and humans. J Clin Invest 2012;122:2176-2194.
25. Alves-Bezerra M, Cohen DE. Triglyceride Metabolism in the Liver. Compr Physiol 2017;8:1-8.
26. Donnelly KL, Smith CI, Schwarzenberg SJ, Jessurun J, Boldt MD, Parks EJ. Sources of fatty acids stored in liver and secreted via lipoproteins in patients with nonalcoholic fatty liver disease. J Clin Invest 2005;115:1343-1351.
27. Pashkov V, Huang J, Parameswara VK, Kedzierski W, Kurrasch DM, Tall GG, Esser V, et al. Regulator of G Protein Signaling (RGS16) Inhibits Hepatic Fatty Acid Oxidation in a Carbohydrate Response Element-binding Protein (ChREBP)-dependent Manner. Journal of Biological Chemistry 2011;286:15116-15125.
28. Jois T, Chen W, Howard V, Harvey R, Youngs K, Thalmann C, Saha P, et al. Deletion of hepatic carbohydrate response element binding protein (ChREBP) impairs glucose homeostasis and hepatic insulin sensitivity in mice. Mol Metab 2017;6:1381-1394.
29. Zhang D, Tong X, VanDommelen K, Gupta N, Stamper K, Brady GF, Meng Z, et al. Lipogenic transcription factor ChREBP mediates fructose-induced metabolic adaptations to prevent hepatotoxicity. J Clin Invest 2017;127:2855-2867.
30. Kim M, Astapova, II, Flier SN, Hannou SA, Doridot L, Sargsyan A, Kou HH, et al. Intestinal, but not hepatic, ChREBP is required for fructose tolerance. JCI Insight 2017;2.
31. Erion DM, Popov V, Hsiao JJ, Vatner D, Mitchell K, Yonemitsu S, Nagai Y, et al. The role of the carbohydrate response element-binding protein in male fructose-fed rats. Endocrinology 2013;154:36-44.
32. Niwa H, Iizuka K, Kato T, Wu W, Tsuchida H, Takao K, Horikawa Y, et al. ChREBP Rather Than SHP Regulates Hepatic VLDL Secretion. Nutrients 2018;10.
33. Wiegman CH, Bandsma RH, Ouwens M, van der Sluijs FH, Havinga R, Boer T, Reijngoud DJ, et al. Hepatic VLDL production in ob/ob mice is not stimulated by massive de novo lipogenesis but is less sensitive to the suppressive effects of insulin. Diabetes 2003;52:1081-1089.
34. Bosy-Westphal A, Braun W, Albrecht V, Muller MJ. Determinants of ectopic liver fat in metabolic disease. Eur J Clin Nutr 2019;73:209-214.

35. **Kooner JS, Chambers JC**, Aguilar-Salinas CA, Hinds DA, Hyde CL, Warnes GR, Perez FJG, et al. Genome-wide scan identifies variation in MLXIPL associated with plasma triglycerides. Nature Genetics 2008;40:149-151.
36. **Willer CJ, Sanna S**, Jackson AU, Scuteri A, Bonnycastle LL, Clarke R, Heath SC, et al. Newly identified loci that influence lipid concentrations and risk of coronary artery disease. Nat Genet 2008;40:161-169.
37. Shaikh S, Waxler JL, Lee H, Grinke K, Garry J, Pober BR, Stanley TL. Glucose and lipid metabolism, bone density, and body composition in individuals with Williams syndrome. Clin Endocrinol (Oxf) 2018;89:596-604.
38. Palacios-Verdu MG, Segura-Puimedon M, Borralleras C, Flores R, Del Campo M, Campuzano V, Perez-Jurado LA. Metabolic abnormalities in Williams-Beuren syndrome. J Med Genet 2015;52:248-255.
39. **Ortega-Azorin C, Sorli JV**, Estruch R, Asensio EM, Coltell O, Gonzalez JI, Martinez-Gonzalez MA, et al. Amino acid change in the carbohydrate response element binding protein is associated with lower triglycerides and myocardial infarction incidence depending on level of adherence to the Mediterranean diet in the PREDIMED trial. Circ Cardiovasc Genet 2014;7:49-58.
40. **Kozlitina J, Smagris E**, Stender S, Nordestgaard BG, Zhou HH, Tybjaerg-Hansen A, Vogt TF, et al. Exome-wide association study identifies a TM6SF2 variant that confers susceptibility to nonalcoholic fatty liver disease. Nat Genet 2014;46:352-356.
41. Smagris E, Gilyard S, BasuRay S, Cohen JC, Hobbs HH. Inactivation of Tm6sf2, a Gene Defective in Fatty Liver Disease, Impairs Lipidation but Not Secretion of Very Low Density Lipoproteins. J Biol Chem 2016;291:10659-10676.
42. Ehrhardt N, Doche ME, Chen S, Mao HZ, Walsh MT, Bedoya C, Guindi M, et al. Hepatic Tm6sf2 overexpression affects cellular ApoB-trafficking, plasma lipid levels, hepatic steatosis and atherosclerosis. Hum Mol Genet 2017;26:2719-2731.
43. **O'Hare EA, Yang R**, Yerges-Armstrong LM, Sreenivasan U, McFarland R, Leitch CC, Wilson MH, et al. TM6SF2 rs58542926 impacts lipid processing in liver and small intestine. Hepatology 2017;65:1526-1542.
44. Mahdessian H, Taxiarchis A, Popov S, Silveira A, Franco-Cereceda A, Hamsten A, Eriksson P, et al. TM6SF2 is a regulator of liver fat metabolism influencing triglyceride secretion and hepatic lipid droplet content. Proc Natl Acad Sci U S A 2014;111:8913-8918.
45. Rajas F, Labrune P, Mithieux G. Glycogen storage disease type 1 and diabetes: learning by comparing and contrasting the two disorders. Diabetes Metab 2013;39:377-387.

46. Oosterveer MH, Schoonjans K. Hepatic glucose sensing and integrative pathways in the liver. Cellular and Molecular Life Sciences 2014;71:1453-1467.
47. Kursawe R, Caprio S, Giannini C, Narayan D, Lin A, D'Adamo E, Shaw M, et al. Decreased transcription of ChREBP-alpha/beta isoforms in abdominal subcutaneous adipose tissue of obese adolescents with prediabetes or early type 2 diabetes: associations with insulin resistance and hyperglycemia. Diabetes 2013;62:837-844.
48. **Eissing L, Scherer T**, Todter K, Knippschild U, Greve JW, Buurman WA, Pinnschmidt HO, et al. De novo lipogenesis in human fat and liver is linked to ChREBP-beta and metabolic health. Nat Commun 2013;4:1528.
49. Holloway MG, Miles GD, Dombkowski AA, Waxman DJ. Liver-specific hepatocyte nuclear factor-4alpha deficiency: greater impact on gene expression in male than in female mouse liver. Mol Endocrinol 2008;22:1274-1286.
50. Oosterveer MH, Grefhorst A, van Dijk TH, Havinga R, Staels B, Kuipers F, Groen AK, et al. Fenofibrate simultaneously induces hepatic fatty acid oxidation, synthesis, and elongation in mice. J Biol Chem 2009;284:34036-34044.

Figure Legends

Figure 1: Hepatic ChREBP knockdown reduces downstream enzymes of glycolysis and increases hepatic G6P and glycogen storage in L-*G6pc*$^{-/-}$ mice. (A) Box and-whisker plots presenting relative hepatic mRNA levels of *Chrebpα* and *Chrebpβ* and relative protein abundance of G6PC and ChREBP in L-*G6pc*$^{+/+}$ and L-*G6pc*$^{-/-}$ treated with either shChREBP or scrambled shRNA (shSCR) (n = 7-9). (B) Heatmaps presenting z-core normalized mRNA expression levels of hepatic glycolysis and pentose phosphate pathway (PPP) enzymes in L-*G6pc*$^{+/+}$ and L-*G6pc*$^{-/-}$ mice treated with shChREBP or shSCR (n = 8-9). (C) Heatmaps presenting z-score normalized hepatic activities of glycolytic enzymes in L-*G6pc*$^{+/+}$ and L-*G6pc*$^{-/-}$ mice treated with shChREBP or shSCR (n = 6). (D) Heatmaps presenting z-score normalized hepatic levels of glycolytic and PPP intermediates in L-*G6pc*$^{+/+}$ and L-*G6pc*$^{-/-}$ mice treated with shChREBP or shSCR (n = 7-9). (E) Box and-whisker plots presenting relative and absolute hepatic glycogen content in L-*G6pc*$^{+/+}$ and L-*G6pc*$^{-/-}$ mice treated with shChREBP or shSCR (n = 7-9).

*p < 0.05, **p <0.01, ***p < 0.001 indicates significance compared to scrambled shRNA. ^p < 0.05, ^^^p <0.001 indicates significance compared to L-*G6pc*$^{+/+}$ mice. Tables S2A-C contain raw values and statistics for data presented in heatmaps.

Figure 2: Hepatic ChREBP knockdown promotes hepatic lipid storage but reduces fractional *de novo* lipogenesis in L-*G6pc*$^{-/-}$ mice. (A) Representative photos of hematoxylin and eosin (H&E) and oil-red-o (ORO) stainings in L-*G6pc*$^{+/+}$ and L-*G6pc*$^{-/-}$ mice treated with either shChREBP or scrambled shRNA (shSCR). (B) Box and-whisker plots presenting hepatic NAFLD Activity Scores (NAS), hepatic lipid droplet sizes and relative and absolute hepatic triglyceride (TG) and cholesteryl ester (CE) contents in L-*G6pc*$^{+/+}$ and L-*G6pc*$^{-/-}$ mice treated with shChREBP or shSCR (n = 6-9). (C) Heatmaps presenting z-score normalized mRNA expression levels of hepatic fatty acid synthesis and TG synthesis enzymes in L-*G6pc*$^{+/+}$ and L-*G6pc*$^{-/-}$ mice treated with shChREBP or shSCR (n = 8-9). (D) Box and-whisker plots presenting fractional acetyl-CoA pool ^{13}C-enrichments in L-*G6pc*$^{+/+}$ and L-*G6pc*$^{-/-}$ mice treated with shChREBP or shSCR (n = 7-9). (E) Box and-whisker plots presenting fractional hepatic *de novo* lipogenesis and fatty acid elongation of pre-existing palmitate in L-*G6pc*$^{+/+}$ and L-*G6pc*$^{-/-}$ mice treated with shChREBP or shSCR (n = 7-9). (F) Box and-whisker plots presenting absolute fatty acid synthesis from *de novo* lipogenesis, chain elongation and the content of old fat in L-*G6pc*$^{+/+}$ and L-*G6pc*$^{-/-}$ mice treated with shChREBP or shSCR (n = 7-9).

*p < 0.05, **p <0.01, ***p < 0.001 indicates significance compared to scrambled shRNA. ^p < 0.05, ^^p < 0.01, ^^^p <0.001 indicates significance compared to L-*G6pc*$^{+/+}$ mice. Table S2A contains raw values and statistics for data presented in heatmaps.

Figure 3: Hepatic ChREBP knockdown strongly suppresses hepatic VLDL-TG secretion by reducing VLDL-TG lipidation. (A) Plasma lipoprotein profiles in L-*G6pc*$^{+/+}$ and L-*G6pc*$^{-/-}$ mice treated with either shChREBP or scrambled shRNA (shSCR). (B) Plasma TG concentrations after P407 injection and box and-whisker plots presenting VLDL-TG secretion rates in L-*G6pc*$^{+/+}$ and L-*G6pc*$^{-/-}$ mice treated with shChREBP or shSCR (n = 4-7). (C) Box and-whisker plots presenting VLDL particle diameter, VLDL particle volume and ratio of TG/apoB48 in L-*G6pc*$^{+/+}$ and L-*G6pc*$^{-/-}$ mice treated with shChREBP or shSCR (n = 3-8).

***p < 0.001 indicates significance compared to scrambled shRNA. ^p < 0.05, ^^p < 0.01 indicates significance compared to L-*G6pc*$^{+/+}$ mice.

Figure 4: Hepatic ChREBP regulates hepatic *Mttp* and *Tm6sf2* expression. (A) Box and-whisker plots presenting hepatic relative levels of VLDL assembly genes in L-*G6pc*$^{+/+}$ and L-*G6pc*$^{-/-}$ mice treated with either shChREBP or scrambled shRNA (shSCR; n = 7-9). (B) Box and-whisker plots presenting hepatic relative abundance of VLDL assembly proteins in L-*G6pc*$^{+/+}$ and L-*G6pc*$^{-/-}$ mice treated with shChREBP or shSCR (n = 6-9). (C) Box and-whisker plots presenting hepatic relative mRNA levels of *Tm6sf2* in L-*G6pc*$^{+/+}$ and S4048 treated mice treated with shChREBP or shSCR (n = 6-7). (D) Schematic presentation of putative ChREBP (#1-4, dark grey) and HNF-4α (DR-1, light grey) response elements within the murine *Tm6sf2* promoter. Box and-whisker plots presenting *in vivo* ChIP analysis of the putative ChREBP response elements in the hepatic *Tm6sf2* promoter in mice treated with shChREBP or shSCR and infused with S4048 or vehicle (n = 5-7). (E) Box and-whisker plots presenting firefly-to-renilla luciferase activities for the murine Tm6sf2 gene reporter after transfection with HNF-4α, MLX, ChREBPα and ChREBPβ plasmids (n = 3-4 independent experiments, each experiment performed in triplicate). (F) Box and-whisker plots presenting *in vivo* ChIP analysis of the putative ChREBP response elements in the hepatic *Tm6sf2* promoter in overnight fasted or fed C57BL6/J mice (n = 5).

*p < 0.05, **p <0.01, ***p < 0.001 indicates significance compared to shSCR for panels A-D, compared to pcDNA3.1 for panel E, and compared to fasted for panel F. ^p < 0.05, ^^p < 0.01, ^^^p <0.001 indicates significance compared to L-*G6pc*$^{+/+}$ mice for panels A-D, compared to control for panel E, and compared to ChREBP for panel F. #p < 0.05, ##p < 0.01 indicates significance compared to pcDNA3.1+HNF-4α for panel E, and compared to fasted for panel F

Table 1. General characteristics and plasma metabolic parameters in L-*G6pc*$^{+/+}$ and L-*G6pc*$^{-/-}$ mice treated with either shChREBP or scrambled shRNA (shSCR).

Data represent median values (range). *p < 0.05, **p <0.01, ***p < 0.001 indicates significance compared to scrambled shRNA. ^p < 0.05, ^^p <0.01, ^^^p <0.001 indicates significance compared to wildtype littermates.

	L-*G6pc*$^{+/+}$ shSCR	L-*G6pc*$^{+/+}$ shChREBP	L-*G6pc*$^{-/-}$ shSCR	L-*G6pc*$^{-/-}$ shChREBP
Body weight (g)	30.0 (28.7 - 35.2)	29.6 (28.5 - 31.4)	30.9 (28.2 - 34.0)	31.3 (28.5 - 34.9)
Food intake (g/day)	3.8 (2.8 - 4.8)	4.3 (3.1 - 5.2)	4.3 (3.2 - 6.0)	4.6 (3.7 - 5.6)
Liver weight (g)	1.6 (1.4 - 2.0)	1.7 (1.6 - 1.9)***	2.4 (1.5 - 2.5)^^^	2.9 (2.7 - 3.5)^^^***
Hepatic protein (mg/g)	138 (113 - 172)	136 (130 - 142)	127 (120 - 141)	112.9 (105.5 - 125.7)^^^***
Hepatic water (%)	68.7 (67.3 - 71.6)	67.5 (65.8 - 69.8)*	67.2 (65.4 - 69.1)^^^	64.9 (62.5 - 65.2)^***
Blood glucose (mmol/L)	9.2 (7.6 - 10.0)	9.4 (8.1 - 10.5)	8.4 (5.2 - 10.7)	6.0 (5.6 - 8.7)**
Plasma insulin (ng/mL)	0.4 (0.2 - 1.1)	0.3 (0.2 - 0.5)	0.4 (0.2 - 1.1)	0.2 (0.1 - 0.3)*
Plasma lactate (mmol/L)	4.4 (4.2 - 5.2)	4.8 (3.3 - 5.6)	6.0 (4.6 - 7.2)^^^	6.2 (5.3 - 7.5)^^^
Plasma ketones (mmol/L)	0.2 (0.1 - 0.2)	0.1 (0.1 - 0.2)	0.2 (0.1 - 0.3)	0.2 (0.1 - 0.3)
Plasma NEFA (µmol/L)	150 (106 - 168)	145 (101 - 190)	247 (141 - 457)^^^	306 (205 - 359)^^^
Plasma TG (mmol/L)	1.2 (1.0 - 1.5)	0.7 (0.5 - 0.9)**	4.3 (1.7 - 5.3)^^^	1.9 (0.2 - 3.3)^^^***
Plasma ALT (U/L)	6 (1 - 10)	3 (1 - 20)	14 (7 - 25)^^	58 (20 - 161)^^^**
Plasma AST (U/L)	25 (19 - 34)	24.(15 - 37)	29 (23 - 48)	46 (28 - 89)^^^*

Table 2. Hepatic fatty acid profile in L-*G6pc*$^{+/+}$ and L-*G6pc*$^{-/-}$ mice treated with either shChREBP or scrambled shRNA (shSCR).

Data represent median values (range). *p < 0.05, **p <0.01, ***p < 0.001 indicates significance compared to scrambled shRNA. ^p < 0.05, ^^p <0.01, ^^^p <0.001 indicates significance compared to wildtype littermates.

nmol/g liver	L-*G6pc*$^{+/+}$ shSCR	L-*G6pc*$^{+/+}$ shChREBP	L-*G6pc*$^{-/-}$ shSCR	L-*G6pc*$^{-/-}$ shChREBP
C14:0	0.4 (0.2 - 0.5)	0.7 (0.4 - 0.8)***	0.6 (0.5 - 0.7)^^^	1.3 (1.0 - 1.4)^^^***
C16:1	2.5 (1.5 - 4.7)	4.0 (1.5 - 5.7)	2.8 (2.3 - 3.6)	6.7 (4.9 - 8.1)^^^***
C16:0	23.3 (15.4 - 29.8)	34.1 (23.8 - 38.0)***	25.8 (19.4 - 29.2)	47.0 (36.4 - 53.0) ^^^***
C18:3ω6	0.1 (0.1 - 0.2)	0.3 (0.2 - 0.4)***	0.2 (0.1 - 0.2)	0.4 (0.3 - 1.0)***
C18:2ω6	14.7 (10.1 - 16.1)	25.3 (15.3 - 29.8)***	16.4 (12.5 - 18.5)	30.7 (21.6 - 38.3)***
C18:3ω3	0.4 (0.3 - 0.5)	0.9 (0.5 - 1.2)***	0.5 (0.3 - 0.7)	1.3 (0.9 - 1.6)^^***
C18:1ω9	24.7 (11.6 - 33.8)	45.2 (21.8 - 49.4)***	46.4 (35.9 - 63.0)^^^	89.8 (64.2 - 111.0)^^^***
C18:1ω7	4.1 (2.2 - 6.6)	5.5 (2.8 - 7.2)	5.7 (4.6 - 6.2)^	9.3 (7.8 - 11.6)^^^***
C18:0	10.2 (6.5 - 12.5)	13.1 (9.5 - 13.9)*	13.7 (12.2 - 15.0)^^^	14.6 (11.8 - 16.4)^^^
C20:4ω6	9.8 (5.7 - 10.3)	10.6 (8.8 - 12.0)	9.3 (8.4 - 11.1)	9.2 (7.9 - 10.7)
C20:5ω3	0.3 (0.2 - 0.3)	0.4 (0.3 - 0.5)*	0.2 (0.2 - 0.4)	0.4 (0.3 - 0.6)***
C20:3ω9	0.3 (0.1 - 0.5)	0.4 (0.2 - 0.6)	0.9 (0.5 -1.1)^^^	0.9 (0.7 - 1.1)^^^
C20:3ω6	1.1 (0.6 - 1.5)	1.4 (1.0 - 1.7)	1.6 (1.3 - 2.0)^^^	2.2 (1.7 - 2.5)^^^**
C20:2ω6	0.2 (0.2 - 0.3)	0.5 (0.3 - 0.5)***	0.3 (0.2 - 0.5)^^	0.7 (0.4 - 0.9)^^***
C20:1ω9	0.4 (0.2 - 0.6)	0.9 (0.5 - 1.2)***	0.9 (0.7 - 1.5)^^^	1.9 (1.4 - 2.7)^^^***
C20:0	0.1 (0.1 - 0.2)	0.2 (0.1 - 0.4)***	0.1 (0.1 - 0.1)	0.2 90.1 - 0.4)***
C22:5ω6	0.2 (0.1 - 0.2)	0.4 (0.2 - 0.5)***	0.4 (0.2 - 0.8)^^^	0.6 (0.3 - 0.8)^*
C22:6ω3	4.3 (2.3 - 5.1)	6.2 (3.9 - 7.0)***	5.3 (3.8 - 5.9)	5.9 (4.3 - 7.6)
C22:4ω6	0.2 (0.1 - 0.3)	0.5 (0.3 - 0.6)***	0.3 (0.2 - 0.5)^	0.7 (0.5 - 0.9)^^^***
C22:5ω3	0.3 (0.1 - 0.4)	0.6 (0.4 - 1.0)***	0.3 (0.2 - 0.4)	1.1 (0.7 - 1.3)^^^***
C22:0	0.3 (0.2 - 0.3)	0.3 (0.2 - 0.4)	0.3 (0.2 - 0.3)	0.3 (0.2 - 0.6)
C24:1ω9	0.4 (0.2 - 0.4)	0.4 (0.4 - 0.5)**	0.4 (0.4 - 0.5)^^	0.4 (0.3 - 0.5)^**
C24:0	0.3 (0.2 - 0.3)	0.3 (0.3 - 0.4)**	0.2 (0.2 - 0.3)^	0.3 (0.3 - 0.3)^^**

Table 3. Hepatic acylcarnitine profile in L-*G6pc*$^{+/+}$ and L-*G6pc*$^{-/-}$ mice treated with either shChREBP or scrambled shRNA (shSCR).

Data represent median values (range). *p < 0.05, **p <0.01 indicates significance compared to scrambled shRNA. ^p < 0.05, ^^p <0.01, ^^^p <0.001 indicates significance compared to wildtype littermates.

µmol/g liver	**L-*G6pc*$^{+/+}$ shSCR**	**L-*G6pc*$^{+/+}$ shChREBP**	**L-*G6pc*$^{-/-}$ shSCR**	**L-*G6pc*$^{-/-}$ shChREBP**
Free carnitine	209 (163 - 324)	241 (172 - 289)	245 (175 - 331)	255 (184 - 289)
C2	35 (12 - 79)	43 (24 - 79)	36 (7 -74)	91 (29 - 122)^*
C3	1.1 (0.7 - 1.9)	1.7 (0.5 - 3.3)	0.5 (0.2 - 0.8)^^^	0.4 (0.0 - 0.9)^^^
C4	0.07 (0.07 -0.33)	0.07 (0.00 - 0.13)	0.37 (0.07 - 1.33)^^^	0.20 (0.07 - 0.40)^^^
C5	0.13 (0.13 - 0.20)	0.23 (0.07 -0.33)	0.23 (0.13 - 0.40)^	0.33 (0.13 - 0.80)
C8	0.13 (0.07 - 0.13)	0.13 (0.07 - 0.13)	0.13 (0.07 - 0.13)	0.13 (0.07 - 0.13)
C10	0.00 (0.00 - 0.07)	0.07 (0.00 - 0.07)	0.07 (0.00 - 0.07)	0.07 (0.00 - 0.07)
C12:1	0.20 (0.07 - 0.33)	0.13 (0.13 - 0.20)	0.17 (0.13 - 0.20)	0.07 (0.07 - 0.13)^^**
C16:1	0.07 (0.00 - 0.07)	0.07 (0.00 -0.07)	0.07 (0.00 - 0.07)	0.00 (0.00 - 0.07)*
C16:0	0.07 (0.07 - 0.20)	0.07 (0.00 - 0.13)	0.07 (0.07 - 0.07)	0.07 (0.00 - 0.07)
C18:2	0.07 (0.07 - 0.13)	0.07 (0.07 - 0.13)	0.07 (0.00 - 0.07)	0.07 (0.00 - 0.07)
C18:1	0.20 (0.07 - 0.33)	0.17 (0.07 - 0.33)	0.13 (0.07 - 0.33)	0.07 (0.07 - 0.13)^^**
C18:0	0.07 (0.07 - 0.13)	0.07 (0.07 - 0.13)	0.07 (0.07 - 0.07)	0.07 (0.00 - 0.07)

Figure 1

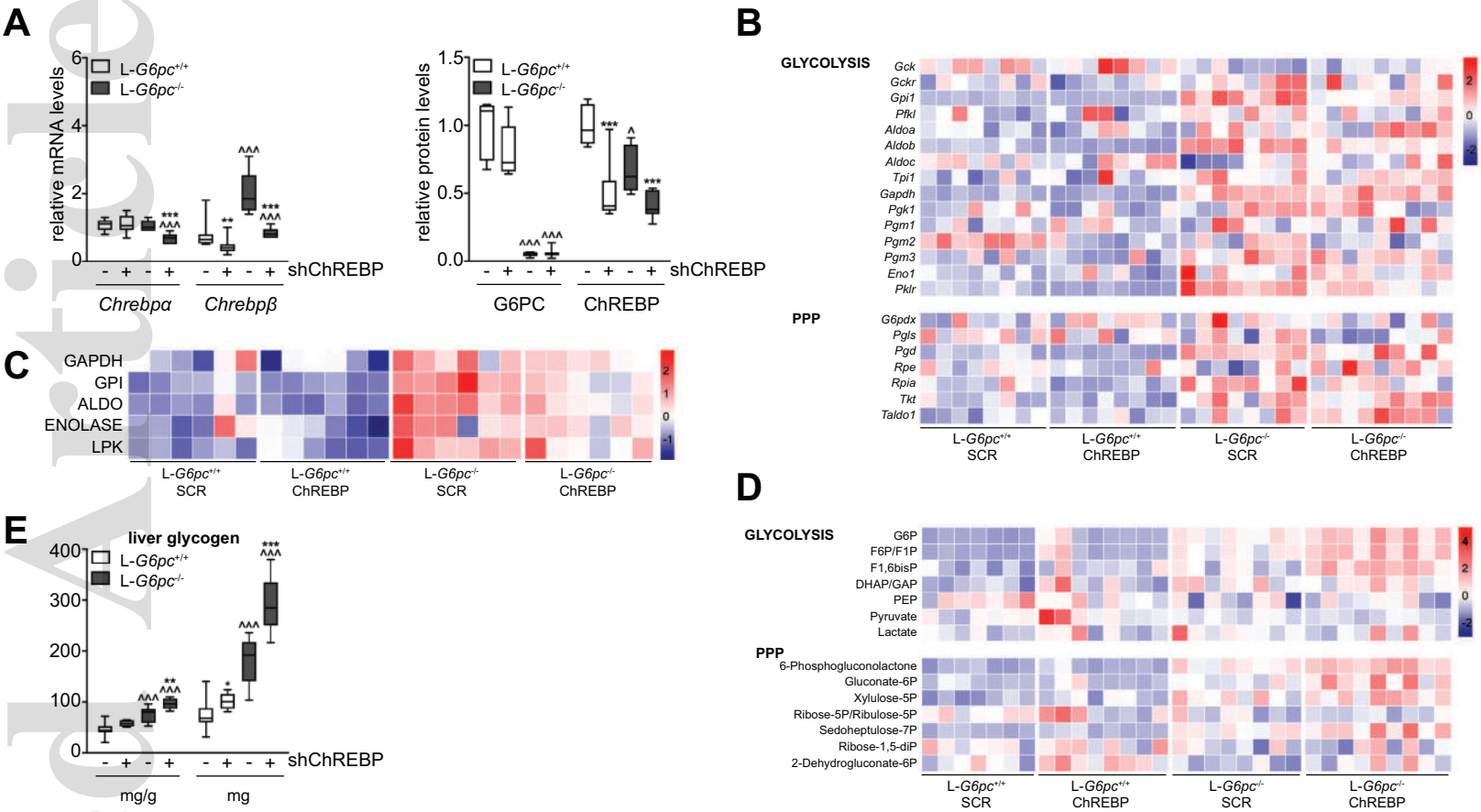

hep_31198_f1.eps

Figure 2

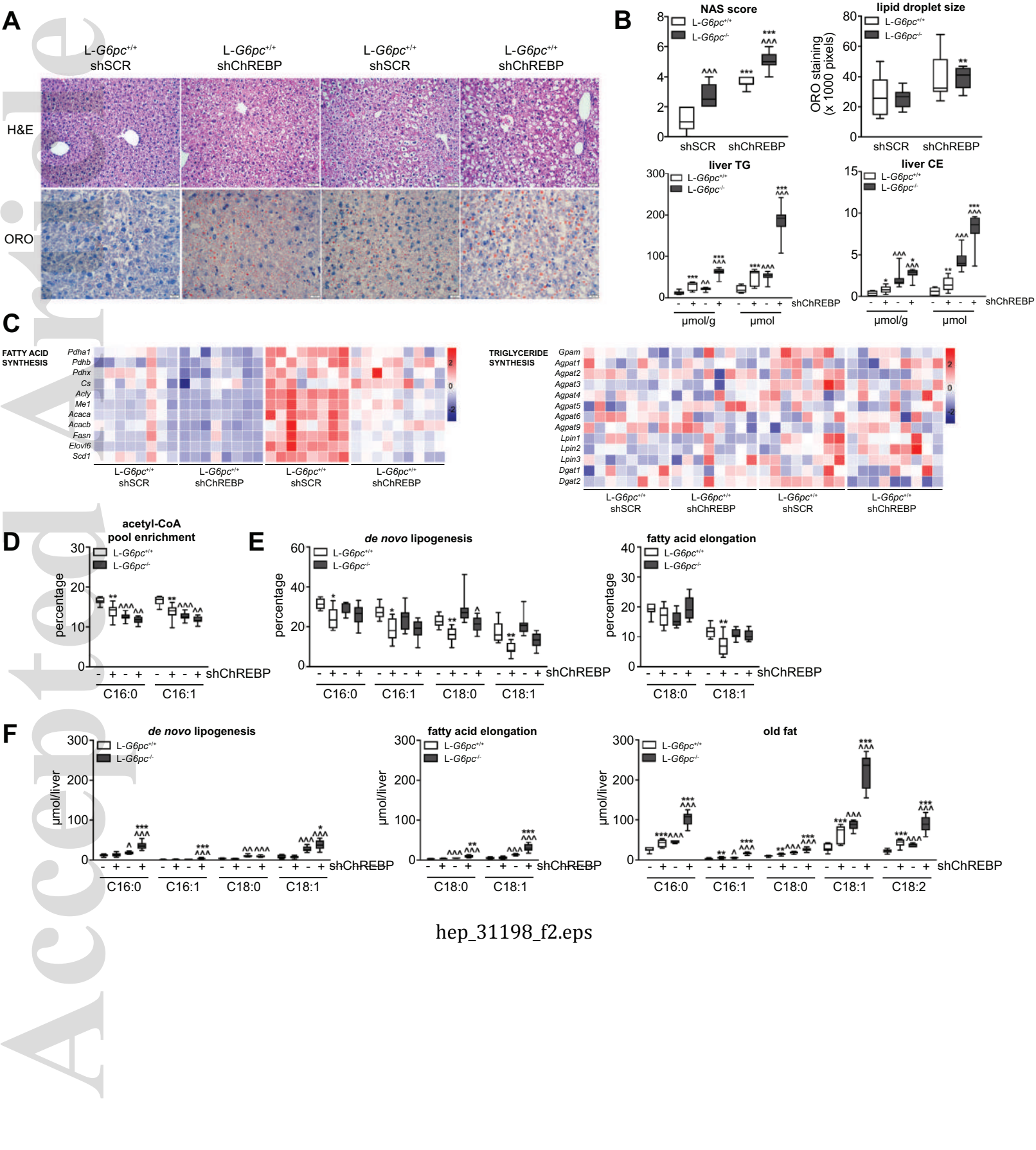

hep_31198_f2.eps

Figure 3

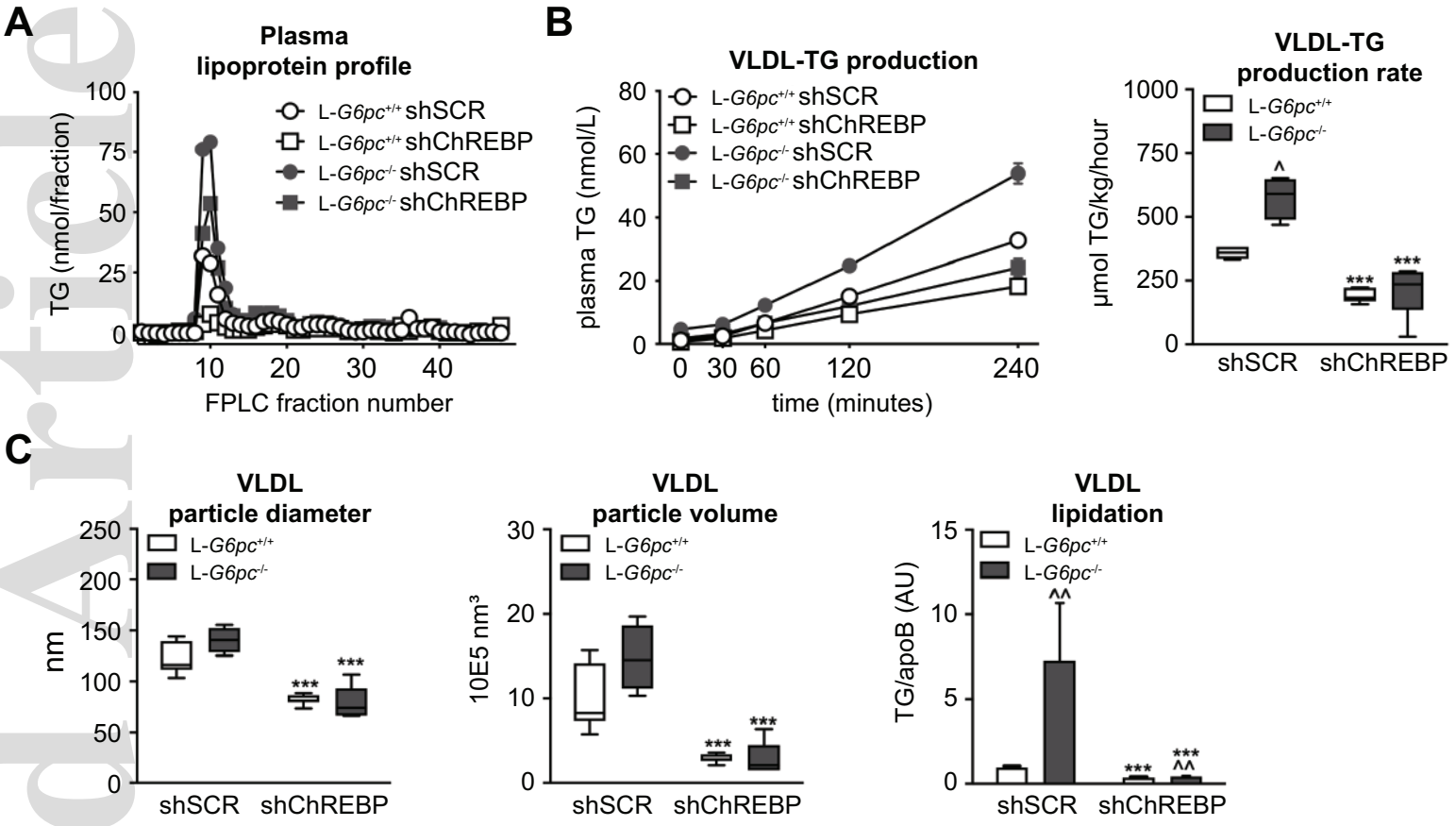

hep_31198_f3.eps

Figure 4

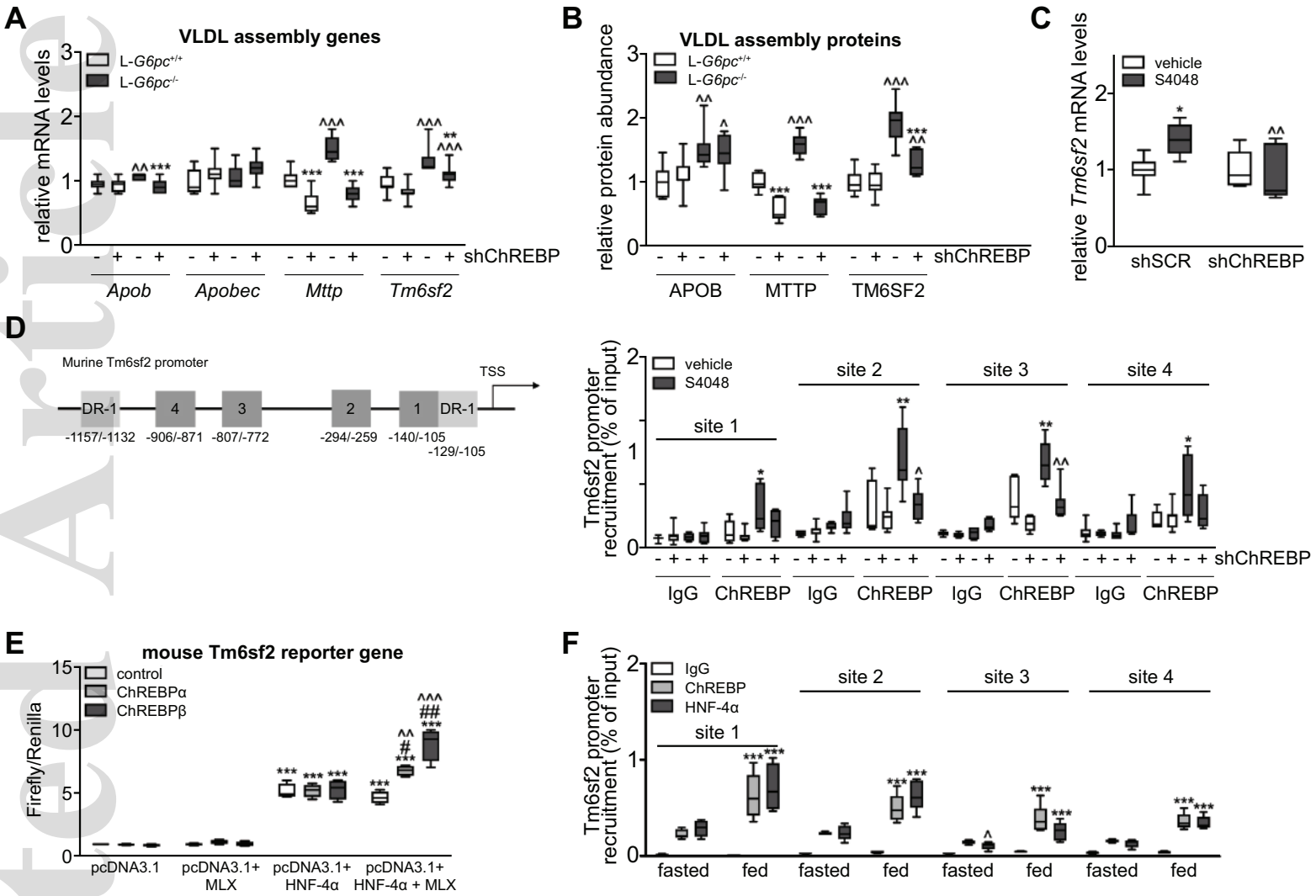

hep_31198_f4.eps